Internal and external forcing of sea level variability in the Black Sea

Denis L. Volkov[1,2*] and Felix W. Landerer[3]

[1]Cooperative Institute for Marine and Atmospheric Studies, University of Miami, Miami, Florida, USA

[2]NOAA-Atlantic Oceanographic and Meteorological Laboratory, Miami, Florida, USA

[3]Jet Propulsion Laboratory, California Institute of Technology, Pasadena, California, USA

*Corresponding author address:
E-mail: denis.volkov@noaa.gov
Tel.: (+1) 305-361-4333

for publication in

Climate Dynamics

Abstract

The variability of sea level in the Black Sea is forced by a combination of internal and external processes of atmospheric, oceanic, and terrestrial origin. We use a combination of satellite altimetry and gravity, tide gauge, river discharge, and atmospheric re-analysis data to provide a comprehensive up-to-date analysis of sea level variability in the Black Sea and to quantify the role of different environmental factors that force the variability. The Black Sea is part of a large-scale climatic system that includes the Mediterranean and the North Atlantic. The seasonal sea level budget shows similar contributions of fresh water fluxes (precipitation, evaporation, and river discharge) and the Black Sea outflow, while the impact of the net surface heat flux is smaller although not negligible. We find that the nonseasonal sea level time series in the Black and Aegean seas are significantly correlated, the latter leading by one month. This lag is attributed to the adjustment of sea level in the Black Sea to externally forced changes of sea level in the Aegean Sea and to the impact of river discharge. The nonseasonal sea level budget in the Black Sea is dominated by precipitation and evaporation over the sea itself, but external processes such as river discharge and changes in the outflow can also cause some large synoptic-scale sea level anomalies. Sea level is strongly coupled to terrestrial water storage over the Black Sea drainage basin, which is modulated by the North Atlantic Oscillation (NAO). We show that during the low/high NAO southwesterly/ northeasterly winds near the Strait of Gibraltar and southerly/northerly winds over the Aegean Sea are able to dynamically increase/decrease sea level in the Mediterranean and Black seas, respectively.

1. Introduction

Sea level is an important parameter that integrates contributions of different environmental processes. Essentially, it is the volume of water that fills a particular basin. The Black Sea is a

rather deep (average depth is 1253 m), almost enclosed basin connected to the Mediterranean Sea by the Turkish Straits System, comprised of the shallow and narrow Straits of Bosphorus and Dardanelles, and the Sea of Marmara (Figure 1). Variations of the basin-averaged sea level in the Black Sea are determined by the basin's freshwater budget, the exchange through the Strait of Bosphorus, and depth-integrated changes in the seawater temperature and salinity.

On average, the excess of precipitation ($Q_P \sim 300$ km^3 yr^{-1}) and river discharge ($Q_R \sim 350$ km^3 yr^{-1}) over evaporation ($Q_E \sim 350$ km^3 yr^{-1}) is balanced by the net outflow ($Q_B \sim 300$ km^3 yr^{-1}) through the Strait of Bosphorus (Ünlüata et al. 1990). The large total freshwater flux relative to the basin volume ($\sim 5.4 \times 10^5$ km^3) makes the Black Sea a typical estuarine basin. The Black Sea drainage basin is the largest in Europe hosting some major European rivers such as Danube, Dnepr, and Don (Figure 1). Its area is several times larger than the Black Sea surface area. This means that large-scale atmospheric processes by means of precipitation and evaporation over land as well as continental discharge have a sizable impact on the Black Sea water balance (Stanev and Peneva 2002).

The average exchange between the Black Sea and the Sea of Marmara is controlled by a two-layer hydraulic transport comprised of the upper layer low-salinity outflow of ~ 600 km^3 yr^{-1} and the lower layer high-salinity inflow of ~ 300 km^3 yr^{-1} (Ünlüata et al. 1990). Recent observations at a number of moorings in the Bosphorus, carried out from September 2008 to February 2009, showed a smaller mean net outflow of over 100 km^3 yr^{-1}; the fluxes in the upper and lower layers were subject to strong variability and coherent with bottom pressure difference along the strait (Jarosz et al. 2011a, 2011b). The exchange across the Bosphorus in response to positive fresh water balance in the Black Sea, the along-strait pressure gradient, and local wind forcing is frequency dependent and strongly nonlinear (Özsoy et al. 1998).

The variability of sea level in the Black Sea observed by tide gauges and satellite altimetry has been described and analyzed in numerous studies. The seasonal cycle and interannual variability are primarily attributed to fresh water fluxes (Boguslavsky et al. 1998; Stanev et al. 2000; Peneva et al. 2001). There are indications that the interannual variability is related to the North Atlantic Oscillation (NAO), the positive/negative phase of which is accompanied by wet/dry climate conditions over northern Europe and dry/wet conditions in southern Europe (Stanev and Peneva 2002). Based on historic measurements at tide gauges from 1873 to 1985, Boguslavsky et al. (1998) estimated a sea level change rate in the Black Sea of 1.6 mm yr^{-1}. Since this rate was similar to the global trend, they concluded that local processes do not play an important role. On the other hand, Tsimplis et al. (2004) observed a trend of 2.2 mm yr^{-1} over the period 1960-2000 and attributed it largely to the surface fresh water flux ($Q_P - Q_E$). Vigo et al. (2005) argued that the thermosteric effect was the major factor for the increase of sea level in the Black Sea from 1993 until the reversal of the trend in mid-1999.

In this paper, we aim to update the analysis of sea level variability in the Black Sea to the near-present time using a combination of satellite altimetry and gravity (GRACE) measurements, available tide gauge and river discharge data, and an atmospheric re-analysis product. Over the period of satellite altimetry observations in the Black Sea from 1992 to present, the record-high sea level anomalies occurred in March 2010, January 2011, and April 2013. A particular emphasis of our study is to understand what processes caused these large anomalies. Hence, our primary focus is on the nonseasonal variability that is the residual signal obtained after the monthly mean climatology has been removed. However, we also consider the seasonal sea level budget to provide a complete scientific view. We discuss the role of different processes of internal and external origin that drive the variability of sea level. Among the internal processes that we consider in this paper

are (i) precipitation (Q_P) and evaporation (Q_E) over the Black Sea, and (ii) the thermal expansion of the Black Sea water. The saline contraction is much smaller than the thermal expansion and thus it is not considered in this study. The external processes include (i) river discharge, which is a function of terrestrial water storage, precipitation (P), and evaporation (E) over the Black Sea drainage basin, (ii) large-scale atmospheric circulation, and (iii) sea level in the Mediterranean and Aegean seas that can change the sea level gradient along the Turkish Straits and thus impact the Black Sea outflow. Although this study is focused on the time interval covered by satellite altimetry observations (1992 – present), we extend our analysis back to 1979, which is limited by the start date of the atmospheric re-analysis product used.

2. Data and Methods

2.1. Satellite Altimetry Data

We use regional weekly maps of sea level anomalies (MSLA) for the Black and Mediterranean Seas, produced by Ssalto/Duacs and distributed by Aviso (www.aviso.oceanobs.com). Each map is generated by merging sea surface height (SSH) measurements from up to four satellites, using all missions available at a given time: Topex/Poseidon, ERS-1/2, Jason-1/2, Envisat, Cryosat-2, and Saral. The SSH records are corrected for instrumental errors, geophysical effects, tidal influence, and atmospheric wind and pressure effects (Le Traon et al. 2003). Sea level anomalies (*SLA*) are calculated by subtracting the 1993-2012 mean profile from SSH and are then mapped on a 1/8°×1/8° regular grid using a method based on a space-time objective analysis that takes into account along-track correlated errors (Le Traon et al. 1998). The *SLA* time series were interpolated at daily time intervals and then monthly averaged to make them consistent with atmospheric data and GRACE.

2.2. Tide Gauge Data

Compared to satellite altimetry, tide gauges provide much longer time series, but lack spatial coverage. We use monthly records from 6 tide gauges – Tuapse, Poti, Trabzon II, Amasra, Igneda, and Constantza (their locations are shown in Figure 1), provided by the Permanent Service for Mean Sea Level (PSMSL, www.psmsl.org). The tide gauges are used to validate satellite altimetry measurements in the Black Sea (see section 2.3) and for extending the sea level record back in time. Table 1 shows the number of the monthly tide gauge records available over the (common with satellite altimetry) 1992-2013 time interval. In the Black Sea, the longest and most up-to-date records available have been obtained at the Poti (Georgia) and Tuapse (Russia) tide gauges. The tide gauge data are corrected for glacial isostatic adjustment (GIA) using the ICE5G_VM2_L90 GIA model (Peltier, 2004). However, the effect of the postglacial rebound in the Black Sea region is very small, and the associated trend does not exceed 0.1 mm/year.

2.3. Comparison of Tide Gauge and Altimetry Data

A dynamic atmospheric correction (DAC) is applied to the Aviso *SLA* products to reduce the aliasing that results from the barotropic response of the ocean to the variable high frequency atmospheric forcing. The DAC is partly derived from a barotropic ocean model forced by the ECMWF (European Centre for Medium Range Weather Forecast) sea surface pressure and wind, MOG2D-G (Lynch and Gray, 1979). It combines the high frequency bands (periods<20 days) from the MOG2D-G model results with the low frequency bands (periods>20 days) from the inverted barometer (IB) correction (Carrere and Lyard 2003). It has been shown that the implementation of DAC improves the quality of altimetry data in coastal regions (Volkov et al. 2007).

Previously, it has been suggested that the IB correction is not necessary in the almost fully isolated Black Sea (Ginzburg et al. 2011), because the atmospheric pressure loading does not

significantly affect the local sea level, as the seawater is virtually incompressible. The IB correction is given by $IB = (P_A - P_{Ref})/\rho g$, where P_A is the sea level pressure (SLP), P_{Ref} is the SLP averaged over the global ocean, ρ is the seawater density, and g is gravity. Since the IB correction is included in DAC, we have tested whether it is appropriate to add the IB correction back to *SLA* records when comparing them to tide gauge measurements. For comparison we computed the root-mean-square (RMS) differences between SLA interpolated onto the tide gauge locations and tide gauge records, RMS (*SLA* – *TG*), and the RMS differences between *SLA* data with the monthly IB correction added back and tide gauge records, RMS (SLA_{+IB}– *TG*), (Table 2). The average RMS difference is 4.9 cm for *SLA*–*TG* and 4.8 cm for SLA_{+IB}–*TG*. This means that adding the IB correction back to *SLA* data does not significantly improve the comparison with tide gauges. Therefore, for our analysis we use the AVISO product without additional modifications.

The RMS difference between *SLA* and the Tuapse tide gauge is about 4 cm. This estimate is close to those obtained in other regions of the World Ocean (e.g. Pascual et al. 2009; Volkov and Pujol 2012). Given that the Tuapse tide gauge provides one of the longest records and thus enables an adequate comparison with satellite altimetry, we will use this record as a proxy for the variability of sea level in the Black Sea dating back to 1979. The correlation coefficient between the tide gauge record at Tuapse and satellite altimetry *SLA* averaged over the entire Black Sea is 0.83.

2.4. Terrestrial Water Storage from GRACE

The GRACE twin-satellites have observed time variations of the Earth's gravity field since May 2002 and provide unique measurements of large-scale monthly mass changes. Most of the monthly gravity changes over land are caused by changes in water storage in hydrologic reservoirs.

Here, we use the new GRACE JPL-RL05M monthly equivalent terrestrial water storage (*TWS*) data derived from the so-called "mascon" approach (Watkins et al., submitted manuscript). This GRACE solution employs global geophysical constraints to invert the GRACE-observations of inter-satellite range rates for monthly gravity changes. These constraints eliminate the need for the otherwise necessary largely empirical post-processing filters that are traditionally applied to reduce noise, but also tend to dampen real geophysical signals (e.g., Landerer and Swenson 2012; Watkins et al., submitted manuscript). The "mascon" solution allows a better separation of land and ocean areas than previous GRACE solutions. The atmospheric mass variations are removed during processing using ECMWF pressure fields, and the remaining mass variations over land are thus mostly related to hydrological processes. We also remove glacial isostatic adjustment effects based on the model of A et al. (2013). Further details on the JPL GRACE-mascon processing can be found in Watkins et al. (submitted manuscript).

2.5. Atmospheric Data

The observed sea level variability is coupled to monthly sea level pressure (*SLP*) and 10 m wind speed data, obtained from the ECMWF's ERA-Interim Re-Analysis (www.ecmwf.net) (Dee et al. 2011). A global mean *SLP* was subtracted from each *SLP* field, because it does not impact sea level. ERA-Interim precipitation and evaporation are used for the analysis of the Black Sea freshwater budget; the net surface heat flux over the Black Sea is used to calculate the thermosteric sea level variability. The ERA-Interim fields are available from January 1979 to the present, which dictates the start date of our analysis.

In addition, we used the monthly North Atlantic Oscillation (NAO) index distributed by the Climate Analysis Section of the National Center for Atmospheric Research (http://climatedataguide.ucar.edu/climate-data/hurrell-north-atlantic-oscillation-nao-index-

station- based, Hurrell 1995). The NAO index is based on the difference of normalized sea level pressure between Lisbon, Portugal and Stykkisholmur/Reykjavik, Iceland. Through fluctuations in this difference the NAO controls the strength and direction of westerly winds and storm tracks over the North Atlantic.

2.6. River Discharge

We use the monthly time series of river discharge at the farthest downstream station of five largest rivers discharging into the Black Sea: Danube, Dnepr, Don, Kuban, and Dnestr (shown in Figure 1). The Danube discharge data are provided by the Global Runoff Data Centre (GRDC, www.bafg.de/GRDC/) and cover the period from January 1931 to December 2010. The discharge data from the remaining 4 rivers come from Dai and Trenberth Global River Flow and Continental Discharge Dataset (DT dataset; Dai and Trenberth 2002; Dai et al. 2009; www.cgd.ucar.edu/cas/catalog/surface/dai-runoff/). The time intervals covered by the available discharge data as well as the mean discharge are summarized in Table 3. All 5 rivers have a common time interval from January 1952 to December 1984 when the integral discharge can be estimated. The Danube River contributes 2/3 of the integral discharge. We regress the Danube discharge onto the integral discharge over the common time interval (1952 – 1984). Then the regression coefficients obtained are used to reconstruct the integral discharge from 1979 to 2010 using the Danube discharge only.

2.7. Identification of Coupled Fields

We used a coupled EOF (cEOF) analysis to identify the temporally co-varying spatial patterns of *SLA*, *TWS*, and *SLP* that explain most of the squared covariance between the field pairs (Bretherton et al. 1992). The temporal evolution of these patterns is demonstrated by two coupled

Principal Component (cPC) time series for each field. Only the first cEOF modes (cEOF-1) are considered in this study. The spatial patterns of cEOF-1 are presented in the form of regression maps obtained by projecting each data field onto its standardized (divided by standard deviation) cPC-1 time series. The regression coefficients are in cm per standard deviation for *SLA* and *TWS*, and in Pa per standard deviation for *SLP*. Regression is also used to examine the structure of wind speed anomalies associated with the cEOF-1 mode of the SLP variability: the zonal and meridional ERA-Interim 10 m wind speed data are projected onto the standardized cPC-1 time series of *SLP* to obtain regression maps of wind vectors. The corresponding regression coefficients are in m s^{-1} (local change in wind speed) per standard deviation change in cPC-1 of *SLP*.

3. Results

3.1. Observed Variability

The variability of sea level in the Black Sea is stronger compared to the Mediterranean. Satellite altimetry observations over 1992-2013 yield the standard deviations of 5.7 cm for *SLA* averaged over the Mediterranean Sea and 7.7 cm for *SLA* averaged over the Black Sea. As illustrated in Figure 2, the *SLA* seasonal cycle (a) is stronger in the Mediterranean Sea, while the *SLA* nonseasonal variability (b) is stronger and dominant in the Black Sea. The standard deviations of the seasonal (nonseasonal) *SLA* averaged over the Mediterranean and Black seas are 5.1 (2.9) cm and 3.1 (6.9) cm, respectively. The nonseasonal variability of *SLA* is almost equally contributed by the intra-seasonal (i.e., synoptic) signals with periods less than one year and interannual variability with periods greater than one year (Figure 2, c and d). The standard deviations of the intra-seasonal and interannual *SLA* averaged over the Black Sea are 4.8 cm and 5.0 cm, respectively.

Displayed in Figure 3 are the time series of *SLA* averaged over 23°E-27°E and 38.5°N-41°N in the Aegean Sea (red curves) and over the Black Sea (black curves). When the monthly mean climatology (seasonal cycle) is removed (Figure 3b), the two time series are significantly correlated at both the interannual and synoptic time scales. The maximum correlation of 0.75 is observed when the nonseasonal variability of *SLA* in the Black Sea lags behind the nonseasonal variability of *SLA* in the Aegean Sea by 1 month. This time lag is especially clear during the winter months of 2009/2010, 2010/2011, and 2012/2013, when the largest anomalies in the satellite altimetry record were observed. Significant correlation suggests that the fluctuations of sea level in one basin are related to the fluctuations in the other. However, it is not clear why the variability in the Black Sea lags behind the variability in the Mediterranean.

It has been reported that the nonseasonal variability of the Mediterranean *SLA* and, in particular, the maxima in two consecutive winters (2009/2010 and 2010/2011) are largely driven by winds just to the west of the Strait of Gibraltar and extending over the strait itself (Landerer and Volkov 2013; Fukumori et al. 2007). The along-strait wind setup forces water into/out of the Mediterranean Sea until the zonal sea level pressure gradient balances the wind stress. This leads to nearly basin-uniform, barotropic changes of the Mediterranean sea level that have been observed independently by satellite altimetry and GRACE (Landerer and Volkov 2013).

3.2. Sea Level Budget

The variability of sea level (η) in the Black Sea can be approximated as follows:

$$\frac{\partial \eta}{\partial t} \cong \frac{\partial \eta_T}{\partial t} + \frac{1}{A_{BS}}(Q_R + Q_P - Q_E - Q_B), \quad (1)$$

where η_T is the thermosteric sea level, Q_R is river discharge, Q_P is precipitation, Q_E is evaporation, Q_B is the net volume flux through the Bosphorus Strait, and A_{BS} is the area of the Black Sea (including the Sea of Azov). Equation (1) does not include the contributions of the halosteric sea level change and groundwater supply. Using salinity fields from an ECCO2 (Estimating the Circulation and Climate of the Ocean, Phase 2) ocean data synthesis product (http://ecco2.jpl.nasa.gov/), we found that the contribution of the halosteric sea level to the total sea level variability is very small (not shown) and can be neglected at the time scales considered (details on estimating steric and halosteric sea level components using ECCO2 data are described in Volkov et al. 2013). The contribution of groundwater is also very likely not significant. Assuming that heat transported by rivers and through the Bosphorus is also small, the time change of the thermosteric sea level is approximately determined by the net surface heat flux, Q_{NET} (positive downward):

$$\frac{\partial \eta_T}{\partial t} \cong \frac{\alpha Q_{\mathrm{NET}}}{\rho C_p}, \tag{2}$$

where $\alpha = 1.3 \times 10^{-4}$ K^{-1} is the thermal expansion coefficient, ρ (= 1018 kg m^{-3}) is the Black Sea water density, and C_P (= 3990 J kg^{-1} K^{-1}) is the seawater specific heat capacity.

The seasonal cycle of the sea level budget components (in cm/month) is displayed in Figure 4. The standard deviation of the seasonal cycle of the Black Sea η is 2.8 cm, which is nearly 3 times smaller than the standard deviation of the total η (7.7 cm). The seasonal maximum of the Black Sea η ($\partial\eta/\partial t$) is observed in June (April-May), while the secondary peak takes place in January (December) (Figure 4a). The seasonal maximum of η in June is mainly caused by the river discharge (blue curves) that peaks in April-May and by evaporation (red curve) that is at a minimum in April. The seasonal cycle of the river discharge is presented for both, the sum of the

six major rivers over the 1952-1985 period (dashed blue curve) and the reconstructed discharge (solid blue curve), which appear to be very close. The contribution of precipitation (green curve) is smaller, but important, because it is responsible for the secondary maximum of η in January. The seasonal amplitude of the thermosteric sea level (dashed black curve) computed using (2) is about 1 cm, and the seasonal maximum occurs in August.

The integral effect of freshwater fluxes and the net surface heat flux is shown in Figure 4b (blue curve). The seasonal amplitude of the associated sea level change is two times greater than the seasonal amplitude of $\partial\eta/\partial t$. This difference must be compensated by the outflow through the Bosphorus Strait (red curve), making the reasonable assumption that the impact of halosteric sea level variability and heat fluxes through river mouths and the Bosphorus Strait are negligible. The outflow in Figure 4b is computed as a residual of the other known terms in equation (1). A caveat of this estimate is that uncertainties in the river runoff and surface freshwater and heat fluxes are also dumped to the outflow. The maximum outflow of about 28 km^3/month equivalent to 6 cm/month sea level change occurs in April-May, while in September-October the net inflow of 9.5 km^3/month balances the sea level decrease due to the negative fresh water flux when evaporation exceeds the sum of precipitation and river discharge.

The annual mean fresh water flux into the Black Sea obtained from ERA-Interim precipitation and evaporation data and river discharge from the DT dataset is about 150 km^3/year, which is balanced by nearly the same outflow. This estimate is two times smaller than the outflow of 300 km^3/year documented by Ünlüata et al. (1990). However, seasonally biased ADCP (Acoustic Doppler Current Profiler) measurements in the Bosphorus Strait carried out from September 2008 to February 2009 revealed a mean net outflow of over 110-120 km^3/year (Jarosz et al. 2011), while the range of the variability exceeded 2000 km^3/year. Unfortunately we cannot estimate the outflow

for exactly the same time interval, because river discharge data are missing in 2010. But using climatological values from September to February we estimate the outflow of about 85 km^3/year, which is below the estimate of Jarosz et al. (2011). The annual mean river discharge is 302 km^3/year, which is close to the 350 km^3/year reported by Ünlüata et al. (1990) taking into account that we used only five major rivers. On the other hand, compared to Ünlüata et al. (1990), the ERA-Interim precipitation is underestimated (~240 km^3/year vs 300 km^3/year) and evaporation is overestimated (~390 km^3/year vs. 350 km^3/year). This can be the reason why the outflow is underestimated in our study.

As mentioned above, the sea level record at the Tuapse tide gauge is a good proxy for the basin-averaged sea level variability in the Black Sea. From this record, we can extend the analysis back to 1979, which is the first year of the ERA-Interim product. The correlation coefficient between the concurrent satellite altimetry sea level averaged over the Black Sea and the Tuapse tide gauge record is 0.83, while the correlation coefficient between their time derivatives is 0.76 (blue and black curves in Figure 5a). When the monthly mean climatology is subtracted from both time series (Figure 5b), the correlation between them remains high: r = 0.82 for the sea level time series and r = 0.72 for their time derivatives. The sum of the thermosteric sea level variability and the freshwater components (red curves in Figure 5) is significantly correlated with the time-derivative of the Tuapse tide gauge record (black curves in Figure 5): r = 0.64 for the initial records and r = 0.43 for the nonseasonal records. However, not all the nonseasonal variability is accounted for by the sum of the thermosteric sea level change and fresh water fluxes. The difference can be due to both the variability of the outflow and errors in the data we used for the budget estimates.

The contribution of the thermosteric sea level variability to the nonseasonal $\partial\eta/\partial t$ in the Black Sea is negligible (Figure 6, green curve). The largest $\partial\eta/\partial t$ contribution comes from other internal

processes: precipitation and evaporation (Figure 6, red curve) together explain 20% of the nonseasonal $\partial\eta/\partial t$ variance. The contribution of the river discharge to the variability of $\partial\eta/\partial t$ is less evident, because it does not explain any $\partial\eta/\partial t$ variance. However, occasional peaks in $\partial\eta/\partial t$ coincide with peaks in the river discharge. Since no river discharge data are available at the end of 2009 and after December 2010, we cannot verify the role of river discharge in generating the observed large anomalies in February 2010, January 2011, and April 2013 independently from GRACE terrestrial water storage data. However, anomalies in Q_P–Q_E (Figure 6, red curve) do not seem to have sufficient magnitude to explain the observed sea level rise; they are also mostly negative. This implies – albeit indirectly – that river discharge and processes that are able to reduce the Black Sea outflow are more likely factors that generated the observed fluctuations.

3.3. Terrestrial Water Storage and River Discharge from GRACE

Terrestrial water storage (*TWS*) over a particular time interval Δt (for GRACE data Δt =1 month) is the time-integral of terrestrial precipitation (*P*) and evaporation (*E*) integrated over the Black Sea drainage basin with an area A_{DB} and the river discharge (Q_R) into the Black Sea:

$$TWS = \frac{1}{A_{DB}} \int (P - E - Q_R) dt \tag{3}$$

GRACE provides monthly mean *TWS* anomalies. Using the estimates of P and E provided by an atmospheric re-analysis product (ERA-Interim in this paper), Q_R can be derived as a residual of equation (3).

Due to measurement uncertainties and monthly discretization of *TWS*, the approximation of its time derivative can introduce considerable high-frequency artifacts (Landerer et al. 2010) in the month-to-month variability of river discharge based on the GRACE *TWS* and the ERA-Interim *P* and *E* data, making these estimates less reliable. Indeed, the monthly time series of the Danube

discharge provided by GRDC and those derived from GRACE and ERA-Interim products are not well correlated (not shown), although yearly averages are well correlated (r = 0.8; Figure 7). Additionally, the annual Danube discharge obtained from GRACE and ERA-Interim data (124 km^3 $year^{-1}$) is strongly underestimated compared to the time-mean of the GRDC data (225 km^3 $year^{-1}$). This bias possibly arises because ERA-Interim underestimates precipitation and overestimates evaporation over some parts of Europe as reported earlier (e.g, Szczypta et al. 2011). Nonetheless, the comparison in Figure 7 demonstrates the potential utility of the GRACE data for recovering the inteannual variability of river discharge into the Black Sea, but a bias correction of about 100 km^3 $year^{-1}$ is necessary when the ERA-Interim P – E is used.

While month-to-month changes of river discharge from GRACE data are problematic as discussed above, we can directly couple monthly *TWS* and the Black Sea *SLA* data using the cEOF analysis. The cEOF-1 mode explains 78% of the squared covariance and demonstrates a strong relationship between the variability of sea level in the Black Sea and the variability of water storage over the Black Sea drainage basin (Figure 8). The correlation coefficient between the cPC-1 time series for *SLA* and *TWS* is 0.77 (Figure 8c). An increase/decrease of *S* over the Black Sea drainage basin (Figure 8b) appears to correspond to an increase/decrease of the Black Sea *SLA* (Figure 8a). It is interesting to note that η and *TWS* are coherent at interannual frequencies. More importantly, however, the large *SLA* anomalies in the Black Sea in December 2002, February 2010, January 2011, and April 2013 are strongly coupled to the associated *TWS* anomalies. Given the fact that *TWS* and *SLA* vary in-phase with little or no lag, we can conclude that (i) river runoff and discharge respond fairly fast to net P – E variations over the drainage areas, and/or (ii) a common external driver like net P – E over both the Black Sea and adjacent land areas are at work. However, since

much of the anomalous *TWS* drains into the Black Sea, we can conclude that the contribution of river discharge to the synoptic *SLA* anomalies is very important.

3.4. Dependence on the Large-Scale Atmospheric Processes

River discharge into the Black Sea is a residual of terrestrial water storage, precipitation, and evaporation over the Black Sea drainage basin. Hence, it depends on large-scale atmospheric processes. To identify the large-scale atmospheric processes linked to the sea level variability in the Black Sea, here we perform cEOF analysis of *TWS* and sea level pressure (*SLP*) over the eastern side of the North Atlantic and Europe (Figure 9). The cEOF-1 mode of *SLP* and *TWS* fields explains 80% of the squared covariance. It exhibits a di-pole SLP pattern with one center located in the eastern North Atlantic near the Azores and another center in the Nordic Seas to the north of Iceland (Figure 9a). This pattern is correlated with an out-of-phase water storage variability highlighting a contrast between southern and northern Europe (Figure 9b). The correlation coefficient between the cPC-1 of *SLP* and *TWS* is 0.54. The low *SLP* anomalies over the eastern North Atlantic are associated with an increase of *TWS*, while the high *SLP* anomalies are related to a decrease of *TWS* in southern Europe, in particular over the Balkans.

The cEOF-1 spatial patterns of *SLP* and *TWS* are in accordance with the North Atlantic Oscillation (NAO), which is a measure of the *SLP* difference between the Azores maximum and Icelandic minimum (Hurrell 1995). Stanev and Peneva (2002) reported a negative correlation between the NAO index and river discharge into the Black Sea. The correlation coefficient between the cPC-1 of *SLP* (red curve in Figure 9c) and the monthly NAO index (grey area in Figure 9c) is – 0.74, while the correlation between the cPC-1 of *TWS* and the monthly NAO index is much lower ($r = –0.35$), but still significant. During times of a high/low NAO index, the axis of the maximum moisture transport shifts northward/southward across the Atlantic and extends over

northern/southern Europe and Scandinavia/Mediterranean Sea. The divergence of moisture transport determines the excess of precipitation over evaporation. As a result, wetter/drier conditions occur over southern Europe and the Mediterranean during the low/high NAO index, while drier/wetter conditions take place over northern Europe. The obtained result suggests that the observed variability of *TWS* over the Black Sea drainage basin is directly linked to large-scale atmospheric processes, modulated by the NAO. Therefore, here we note that the observed maxima of *TWS* in winters 2009/2010 and 2010/2011 are related to strongly negative NAO indices (Figure 9c).

Displayed in Figure 10 is the result of the coupling of *SLA* with *SLP* and wind speed. The cEOF-1 mode explains 92% of the squared covariance between the *SLA* and *SLP* fields. The regression map of SSH exhibits a basin-scale oscillation pattern that extends over the entire Mediterranean and Black Seas (Figure 10a). The *SLA* pattern in the Mediterranean Sea is similar to the one reported earlier by Landerer and Volkov (2013). By including the Black Sea in the cEOF analysis, we observe that the Black Sea is the region where the maximum fluctuations of *SLA* in relation with the large-scale *SLP* fluctuations take place. If the cEOF analysis is conducted for $\partial\eta/\partial t$ and *SLP* (not shown), then the Black Sea stands out as the only region where $\partial\eta/\partial t$ is statistically related to *SLP* changes. This is expected due to the observed time lag between the basin-averaged sea levels in the Black and Aegean Seas (Figure 3). With regard to the Mediterranean, the barotropic response of the Mediterranean sea level to wind forcing near the Strait of Gibraltar (Landerer and Volkov 2013) is so fast that it is shown to be simultaneous in monthly data.

The regression map of *SLP* demonstrates a di-pole oscillating pattern (Figure 10b), similar to cEOF-1 mode of *SLP* coupled to the terrestrial water storage (Figure 9a). The correlation

coefficient between the cPC-1 time series of *SLA* and *SLP* is 0.62 (Figure 10c). Large synoptic fluctuations of cPC-1 of *SLP* in winters 2009/2010, 2010/2011, and 2012/2013 are correlated with corresponding fluctuations of cPC-1 of *SLA*. The correlation coefficients between the cPC-1 of *SLP/SLA* and the monthly NAO index is -0.77 / –0.42, which indicates that sea level in both the Mediterranean and Black Seas is linked to the NAO. The influence of the NAO on the Mediterranean sea level over longer time scales has been related to the atmospheric pressure loading and also to the local changes in precipitation and evaporation (Tsimplis and Josey 2001). The NAO has also been found to indirectly affect the synoptic variability of the Mediterranean sea level (Landerer and Volkov 2013). Our results here demonstrate that the NAO impact is also relevant for the synoptic variability of sea level in the Black Sea.

3.5. The Role of Wind Forcing

As discussed above, the variability of *TWS* over the Black Sea drainage basin – and thus also river discharge – is one of the important sources for sea level anomalies in the Black Sea. Another mechanism can be linked to wind forcing that can impact the Black Sea outflow. Displayed in Figure 10b is the regression map of ERA-Interim winds projected on cPC-1 of *SLP* (Figure 10c, red curve); Figure 10d shows a zoom-in for the eastern Mediterranean and the Black Sea region. The displayed wind pattern is in accordance with the low NAO index and features weak westerly winds over the North Atlantic Ocean. During the times of low/high NAO, the northeastward/southwestward wind anomalies occur near the Strait of Gibraltar. These wind anomalies contribute to the along-strait wind that leads to barotropic fluctuations of the Mediterranean sea level (Landerer and Volkov 2013; Fukumori et al. 2007). At the same time, the NAO also determines the strongest meridional wind anomalies over the eastern Mediterranean and along the Aegean Sea (Figure 10d): the low/high NAO is associated with a strong

northward/southward wind over the Aegean Sea and an increase/decrease of sea level in the Black Sea. Strong winds are able to significantly reduce the Black Sea outflow or even reverse the net volume flux (Jarosz et al. 2011). Thus, our analysis suggests that the NAO-modulated wind over the Aegean Sea may be another factor that influences the variability of sea level in the Black Sea at both the synoptic and interannual time scales.

4. Discussion and Conclusions

In this study, we have reported on a lagged correlation between the nonseasonal fluctuations of *SLA* in the Aegean Sea (extending into the entire Mediterranean) and in the Black Sea; the Aegean mean *SLA* leads the Black Sea mean *SLA* by 1 month. This observation sheds new light on the role of external processes that may affect the variability of the Black Sea *SLA*, besides precipitation and evaporation over the Black Sea itself and the adjacent drainage area. The time lag is consistent over the observational time period. This fact rejects the possibility that the Black Sea outflow significantly contributes to the Mediterranean sea level variability, for example, in the case when the outflow is retained in the eastern Mediterranean by wind. We suggest two hypotheses that can explain the time lag.

The first hypothesis is that the time lag is due to local differences in the role of fresh water fluxes. Unlike the Mediterranean, the Black Sea is strongly influenced by river discharge, and because of the positive fresh water balance it eventually outflows into the Mediterranean Sea. On the one hand, the maximum precipitation in both basins takes place in the winter months, which coincides with the times when the largest peaks are observed (Figure 3). On the other hand, the maximum river discharge in the Black Sea typically occurs in spring (Figure 4a), and it can be responsible for the time lag between the maximum sea levels in both seas and for the larger amplitude of sea level fluctuations in the Black Sea. Supporting this argument, we have shown

that the nonseasonal variability of *SLA* in the Black Sea, including the synoptic anomalies in February 2010, January 2011, and April 2013, is coupled to terrestrial water storage variability of the Black Sea drainage basin (Figure 8). This means that river discharge, which is the residual of the land water storage change, precipitation, and evaporation, was one of the factors that contributed to the observed synoptic and interannual sea level fluctuations. The dominant mode of the terrestrial water storage and thus river discharge variability is related to the NAO (Figure 9). Nevertheless, the first hypothesis assumes that the observed large fluctuations of sea level in 2010, 2011, and 2013 (Figure 3) were driven by freshwater fluxes in both the Mediterranean and Black Seas, but it has been shown that the first two anomalies in the Mediterranean Sea were related to wind forcing near the Strait of Gibraltar (Landerer and Volkov 2013). A detailed assessment of the impact of freshwater fluxes on the Mediterranean sea level would help to validate this hypothesis.

The second, and more likely, hypothesis is that the barotropic, basin-wide sea level fluctuations in the Mediterranean Sea, forced by winds near the Strait of Gibraltar (Fukumori et al. 2007; Menemenlis et al. 2007; Landerer and Volkov 2013), lead to changes in the sea level gradient between the Aegean and Black Seas and, consequently, modify the volume of the Black Sea outflow. In a balanced mean state, the Black Sea outflow balances the positive fresh water budget ($Q_P–Q_E+Q_R$) of the Black Sea. If we assume a constant $Q_P–Q_E+Q_R$ in the Black Sea, then, as sea level in the Aegean Sea increases, the Black Sea outflow (Q_B) must decrease. As a result, sea level in the Black Sea will start rising until the sea level gradient between the Aegean and Black Seas is re-established to balance the inflow of fresh water into the Black Sea. If this scenario is correct, then the observed one-month lag is the time required for the Black Sea *SLA* to adjust to the

Mediterranean *SLA*. The relevance of the second hypothesis can be investigated by conducting dedicated regional numerical experiments, which is the subject of future work.

Our study has demonstrated that atmospheric circulation patterns near the Strait of Gibraltar and over the Aegean Sea, which are modulated by the NAO, can also be responsible for the observed *SLA* variability in both the Mediterranean and Black Seas. During the times of low/high NAO, southwesterly/northeasterly winds over the Strait of Gibraltar cause an increase/decrease of the basin-wide Mediterranean sea level (Figure 10). This process, reported earlier by Fukumori et al. (2007) and Landerer and Volkov (2013), leads to a change in the sea level gradient between the Black and Aegean Seas and, consequently, affects the Black Sea outflow. In addition, the low/high NAO periods are associated with northerly/southerly wind anomalies over the Aegean Sea (Figure 10). These winds can amplify the local sea level changes and significantly impact the Black Sea outflow. For example, the strong northerly winds over the Aegean Sea and the Turkish Straits can significantly reduce or even reverse the Black Sea outflow.

The major conclusions of our study can be summarized as follows:

1. Satellite altimetry and tide gauges have observed strong fluctuations of *SLA* in the Black Sea with very high anomalies in February 2010, January 2011, and April 2013. Compared to the Mediterranean, the seasonal cycle of *SLA* in the Black Sea is relatively small and the variability is dominated by the nonseasonal signals.
2. The time series of the nonseasonal *SLA* in the Black and the Aegean Seas are correlated; the Black Sea *SLA* lags behind the Aegean Sea *SLA* by one month, which suggests an influence of external dynamic processes on *SLA* in the Black Sea.

3. The seasonal sea level budget shows comparable contributions of precipitation and evaporation over the Black Sea (internal processes), river discharge and outflow (external processes); the impact of the surface heat flux (internal process) is rather small with an amplitude of 1 cm.
4. The nonseasonal sea level budget is dominated by freshwater fluxes and suggests that external processes such as river discharge and changes in the outflow can be responsible for the observed large anomalies in February 2010, January 2011, and April 2013. We find a strong correlation between the nonseasonal SLA in the Black Sea and the nonseasonal terrestrial water storage over the Black Sea drainage basin, which also indicates that the contribution of river discharge to large anomalies in February 2010, January 2011, and April 2013 is important.
5. We demonstrate that the GRACE observations can be used to study the interannual variability of river discharge into the Black Sea; however, the synoptic variability is contaminated by high frequency artifacts.
6. Water storage anomalies over the Black Sea drainage basin are caused by precipitation and evaporation fluctuations that are dependent on the large-scale atmospheric circulation pattern modulated by the NAO.
7. The NAO-related large-scale atmospheric circulation drives the sea level variability over the Mediterranean and Black Seas by means of wind forcing near the Strait of Gibraltar and over the Aegean Sea and Turkish Straits, respectively.

Acknowledgments

The satellite altimetry SLA data were produced by Ssalto/Duacs and distributed by Aviso (www.aviso.oceanobs.com) with support from CNES. GRACE land data (available at http://grace.jpl.nasa.gov) and supported by the NASA MEaSUREs Program. We thank the Global Runoff Data Centre for kindly providing us the Danube discharge time series. The authors thank Sang-Ki Lee, Elizabeth Johns, and an anonymous reviewer for valuable comments on the initial version of the manuscript. This research was funded by the NASA Ocean Surface Topography Science Team program (grant number NNX13AO73G) and carried out at NOAA Atlantic Oceanographic and Meteorological Laboratory and Jet Propulsion Laboratory, California Institute of Technology.

References

A, G., J. Wahr, and S. Zhong (2013), Coputations of the viscoelastic response of a 3-D compressible Earth to surface loading: an application to Glacial Isostatic Adjustment in Antarctica and Canada, *Geophys. J. Int.*, 192, 557-572, doi:10.1093/gji/ggs030.

Boguslavsky, S.G., A.I. Kubryakov, and I.K. Ivashchenko (1998), Variations of the Black Sea level, *Phys. Oceanogr*., Vol.9, 3, 199-208.

Bretherton, C.S., C. Smith, and J.M. Wallace (1992), An intercomparison of methods for finding coupled patterns in climate data, *J. Clim*., 5, 541-560.

Carrere, L., and F. Lyard (2003), Modeling the barotropic response of the global ocean to atmospheric wind and pressure forcing: Comparisons with observations, *Geophys. Res. Lett.*, 30(6), 1275, doi:10.1029/ 2002GL016473.

Dai, A., T. Qian, K. E. Trenberth, and J. D Milliman (2009), Changes in continental freshwater discharge from 1948-2004. *J. Climate*, **22,** 2773-2791.

Dai, A., and K. E. Trenberth (2002), Estimates of freshwater discharge from continents: latitudinal and seasonal variations. *J. Hydrometeorol.*, **3**, 660-687.

Dee, D. P., et al. (2011), The ERA-Interim reanalysis: configuration and performance of the data assimilation system, *Quarterly Journal of the Royal Meteorological Society, John Wiley & Sons, Ltd., 137*, 553-597.

Fukumori, I., D. Menemenlis, *and* T. Lee *(*2007*),* A near-uniform basin-wide sea level fluctuation of the Mediterranean Sea, *J. Phys. Oceanogr.*, 37*(*2*),* 338–358.

Ginzburg, A.I., A.G. Kostianoy, N.A. Sheremet, and S.A. Lebedev (2011), Satellite altimetry applications in the Black Sea, In: *Coastal Altimetry*, Vignudelli et al. Eds., Springer-Verlag, Berlin Heidelberg, 565 pp.

Hurrell, J.W. (1995), Decadal Trends in the North Atlantic Oscillation: Regional Temperatures and Precipitation, *Science*, Vol. 269, pp.676-679.

Jarosz, E., W. J. Teague, J. W. Book, and S. Besiktepe (2011a), Observed volume fluxes in the Bosphorus Strait, *Geophys. Res. Lett*., 38, L21608, doi:10.1029/ 2011GL049557.

Jarosz, E., W. J. Teague, J. W. Book, and S. Besiktepe (2011), On flow variability in the Bosphorus Strait, *J. Geophys. Res.*, 116, C08038, doi:10.1029/2010JC006861.

Landerer, F. W., *and* D. L. Volkov *(*2013*),* The anatomy of recent large sea level fluctuations in the Mediterranean Sea, *Geophys. Res. Lett.*, 40, 553–557, *doi:10.1002/grl.50140.*

Landerer, F.W. and S. C. Swenson (2012), Accuracy of scaled GRACE terrestrial water storage estimates, *Water Resources Research*, Vol 48, W04531, 11 PP, doi:10.1029/2011WR011453.

Landerer, F.W., J.O. Dickey, and A. Guntner (2010), Terrestrial water budget of the Eurasian pan-Arctic from GRACE satellite measurements during 2003-2009, *J. Geophys. Res.*, 115, D23115, doi:10.1029/2010JD014584.

Le Traon, P. Y., Y. Faugère, F. Hernandez, J. Dorandeu, F. Mertz, M. Ablain (2003), Can We Merge GEOSAT Follow-On with TOPEX/Poseidon and ERS-2 for an Improved Description of the Ocean Circulation?, *J. Atmos. Oceanic Technol.*, **20**, 889–895, doi: http://dx.doi.org/10.1175/1520-0426(2003)020<0889:CWMGFW>2.0.CO;2.

Le Traon, P. Y., F. Nadal, and N. Ducet (1998), An Improved Mapping Method of Multisatellite Altimeter Data. *J. Atmos. Oceanic Technol.*, **15**, 522–534, doi: http://dx.doi.org/10.1175/1520-0426(1998)015<0522:AIMMOM>2.0.CO;2.

Lynch, D. R., and W. G. Gray (1979), A wave equation model for finite element tidal computations, *Comput. Fluids*, 7, 207–228, doi:10.1016/0045-7930(79)90037-9.

Menemenlis, D., I. Fukumori, *and* T. Lee *(*2007*),* Atlantic to Mediterranean sea level difference driven by winds near Gibraltar strait, *J. Phys. Oceangr.*, 37, 359, *doi:10.1175/JPO3015.1.*

Özsoy, E., M.A. Latif, S.T. Besiktepe, N. Cetin, M.C. Gregg, V. Belokopytov, Y. Goryachkin, and V. Diaconu (1998), The Bosphorus Strait: exchange fluxes, currents, and sea level changes, In: Ecosystem Modeling as a Management Tool for the Black Sea, NATO Sci. Ser. 2, Environ. Security, vol.47, edited by L. Ivanov and T. Oguz, pp. 1-27, Kluwer Acad., Dordrecht, Netherlands.

Pascual, A., C. Boone, G. Larnicol, and P.-Y. Le Traon (2009), On the qual- ity of real-time altimeter gridded fields: Comparison with in situ data, *J. Atmos. Oceanic Technol.*, 26, 556–569, doi:10.1175/2008JTECHO556.1.

Peltier, W. R. (2004), Global glacial isostasy and the surface of the Ice-Age Earth: The ICE-5G(VM2) model and GRACE, Annu. Rev. Earth Planet. Sci., 32, 111–149, doi:10.1146/annurev.earth.32.082503.144359.

Peneva, E., E. Stanev, V. Belokopytov, and P.-Y. Le Traon (2001), Water transport in the Bosphorus Straits estimated from hydro-meteorological and altimeter data: seasonal to decadal variability, *J. Marine Sys.*, 31, 21-33.

Stanev, J.V., and E.L. Peneva (2002), Regional response to global climatic change: Black Sea examples, *Global Planet. Change*, 32, 33-47.

Stanev, E.V., P-Y. Le Traon, and E.L. Peneva (2000), Sea level variations and their dependency on meteorological and hydrological forcing: analysis of altimeter and surface data for the Black Sea, *J. Geophys. Res.*, 105, C7, 17203-17216.

Swenson, S. C. and J. Wahr (2006), Post-processing removal of correlated errors in GRACE data, *Geophys. Res. Lett.*, 33, L08402, doi:10.1029/2005GL025285.

Szczypta, C., J.-C. Calvet, C. Albergel, G. Balsamo, S. Boussetta, D. Carrer, S. Lafont, and C. Meurey (2011), Verification of the new ECMWF ERA-Interim reanalysis over France, *Hydrol. Earth Syst. Sci.*, 15, 647-666, doi:10.5194/hess-15-647-2011.

Tsimplis, M.N., S.A. Josey, M. Rixen, and E.V. Stanev (2004), On the forcing of sea level in the Black Sea, *J. Geophys. Res.*, 109, C08015, doi:10.1029/2003JC002185.

Ünlüata, U., T. Oguz, M.A. Latif, and E. Özsoy (1990), On the physical oceanography of the Turkish Straiits. In: Pratt, G. (Ed.), The Physical Oceanography of Sea Straits. NATO ASI Ser., Ser. C., Kluwer Academic Publishing, Norwell, MA, pp. 25-60.

Vigo, I., D. Garcia, and B.F. Chao (2005), Change of sea level trend in the Mediterranean and Black sea, *J. Marine Res.*, 63, 1085-1100.

Volkov, D.L., F.W. Landerer, and S.A. Kirillov (2013), The genesis of sea level variability in the Barents Sea, *Continental Shelf. Res.*, 66, 92-104, doi:10.1016/j.csr.2013.07.007.

Volkov, D. L., and M.-I. Pujol (2012), Quality assessment of a satellite altimetry data product in the Nordic, Barents, and Kara seas, *J. Geophys. Res.*, 117, C03025, doi:10.1029/2011JC007557.

Volkov, D.L., G. Larnicol, and J. Dorandeu (2007), Improving the quality of satellite altimetry data over continental shelves, *J. Geophys. Res.*, 112, C06020, doi:10.1029/2006JC003765.

Watkins, M.M., D. N. Wiese, D.-N. Yuan, C. Boening, and F.W. Landerer (2014), Improved Methods for Observing Earth's Time Variable Mass Distribution with GRACE, *J. Geophys. Res.* (submitted manuscript).

Table 1. The list of tide gauges used for comparison with satellite altimetry and the number of records during the 1992-2013 time interval.

Tide Gauge	*Country*	*Number of Monthly Records in 1992-2013*
Tuapse	Russia	237
Poti	Georgia	251
Trabzon II	Turkey	80
Amasra	Turkey	97
Igneda	Turkey	83
Constantza	Romania	66

Table 2. RMS differences (cm) between the original AVISO and tide gauge SLA and between the AVISO SLA with IB correction added back and tide gauge SLA.

Tide Gauge	*RMS (SLA – TG)*	*RMS (SLA_{+IB} – TG)*
Tuapse	4.3	4.2
Poti	6.7	7.5
Trabzon II	4.2	2.6
Amasra	4.5	5.3
Igneda	4.6	4.0
Constantza	5.0	5.2

Table 3. The largest rivers discharging into the Black Sea, the time intervals of data availability, and the time mean discharge.

River	*Time interval*	*Mean discharge ($km^3\ yr^{-1}$)*
Danube	1931 – 2010	206
Dnepr	1952 – 1984	47
Don	1931 – 1995	24
Kuban	1931 – 1998	12
Dnestr	1945 – 1985	10
Sum of 5 rivers	1952 – 1984	302

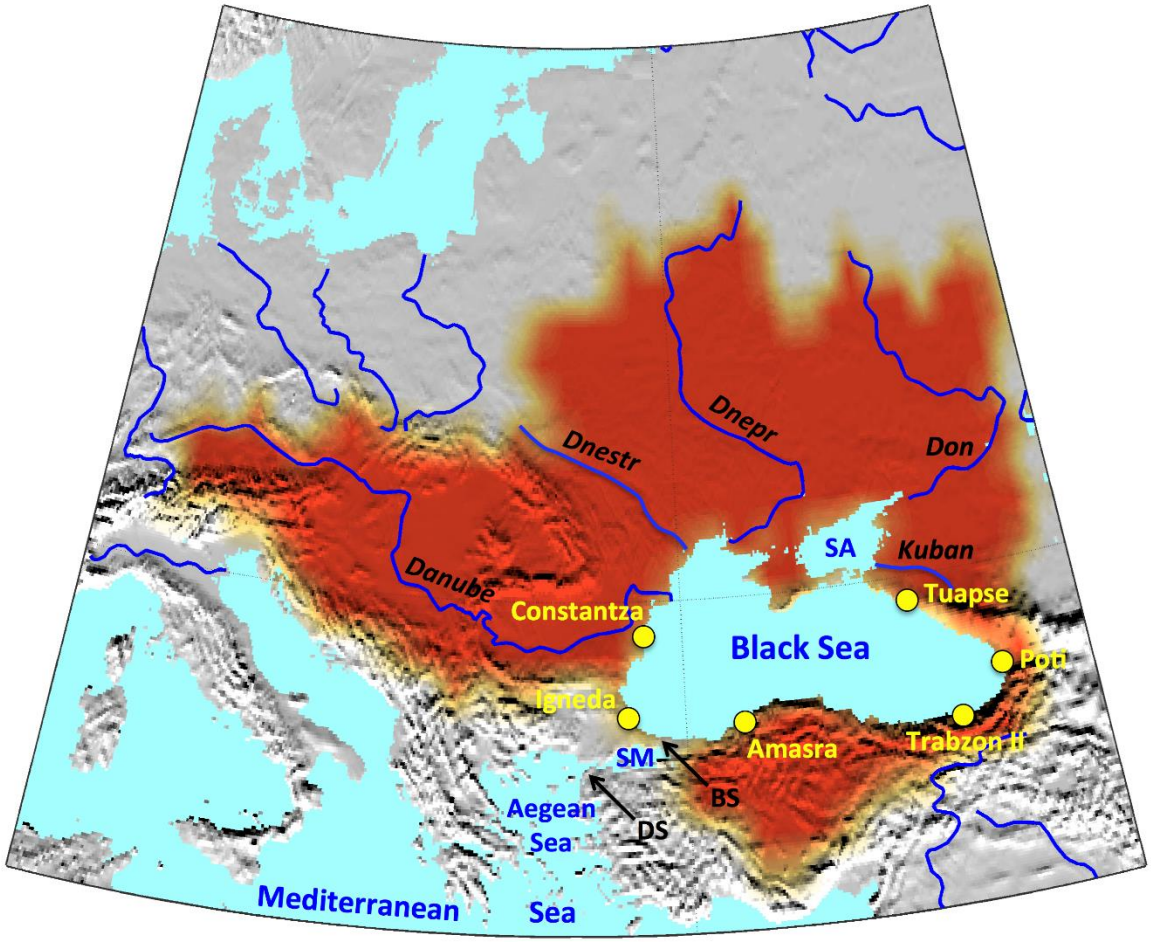

Figure 1. The Black Sea drainage basin (colored area), the largest rivers, and the locations of tide gauges used for the analysis (yellow circles). Abbreviations: BS–Bosphorus Strait, DS–Dardanelles Strait, SA–the Sea of Azov, and SM–the Sea of Marmara.

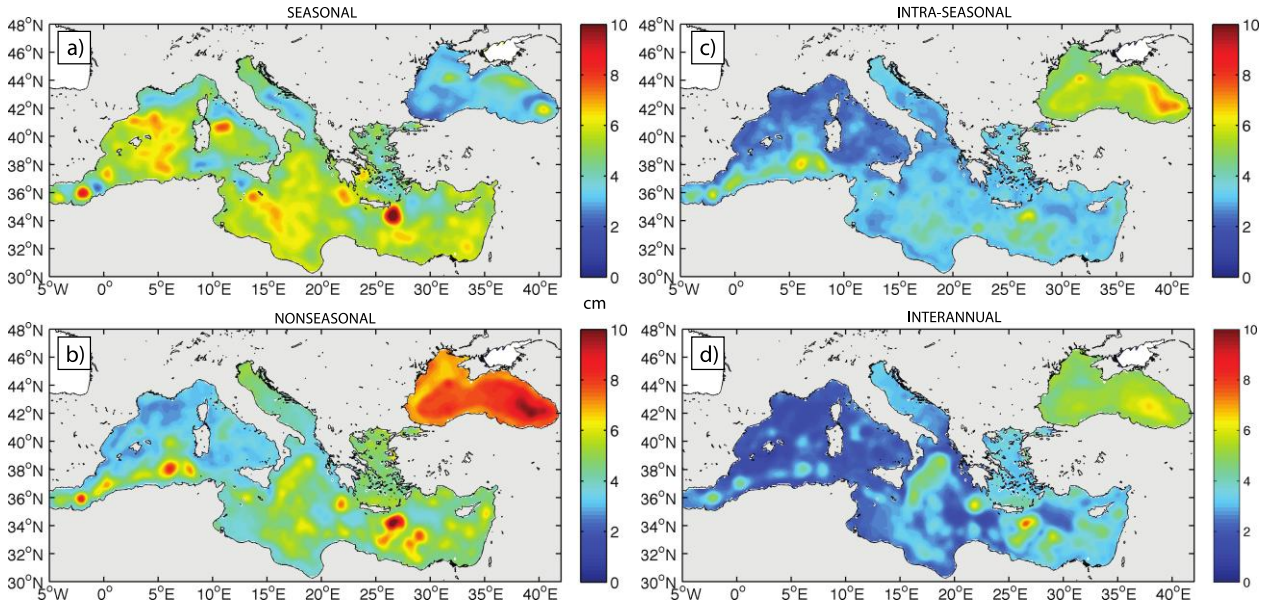

Figure 2. Standard deviations of *SLA*: (a) seasonal cycle, (b) nonseasonal variability (after the seasonal cycle has been removed), (c) intra-seasonal signals, and (d) interannual signals.

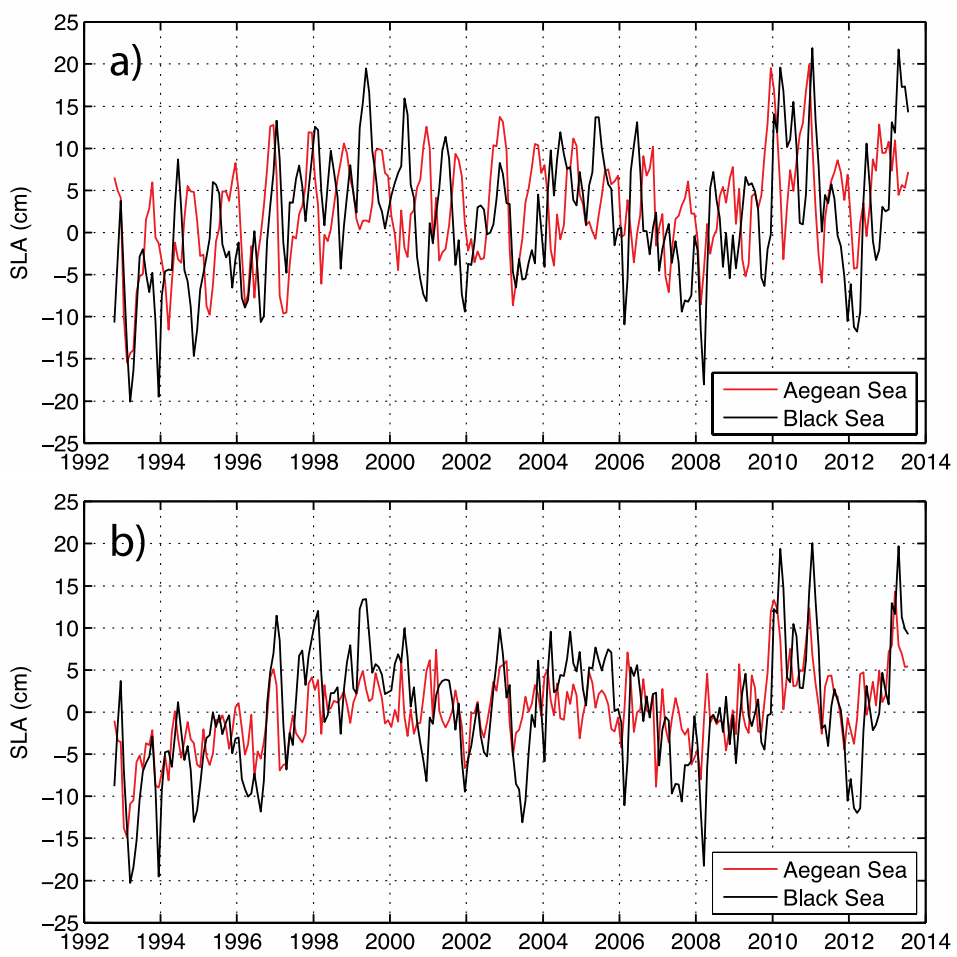

Figure 3. The time series of *SLA* averaged over the Black (black) and Aegean (red) Seas: (a) seasonal cycle is present; and (b) seasonal cycle is removed. Maximum correlation between the time series is 0.75 at 1 month time lag (see Figure 4).

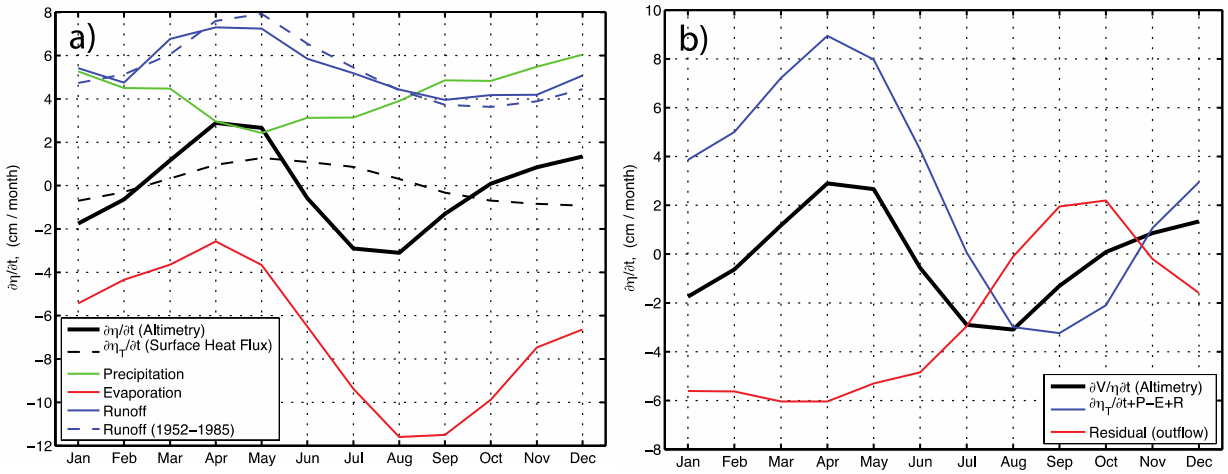

Figure 4. The seasonal cycle (monthly mean climatology) of *SLA* change components in the Black Sea: (a) the total *SLA* change (bold black), *SLA* change due to surface heat flux (dashed black), *SLA* change due to precipitation (green), *SLA* change due to evaporation (red), *SLA* change due to river discharge (blue), *SLA* change due to river discharge over the 1952-1985 period when the discharge data of 5 largest rivers (Danube, Dnepr, Dnestr, Don, Kuban) are available (dashed blue); (b) the total *SLA* change (bold black), the integral *SLA* change due to surface heat flux, precipitation, evaporation and river discharge (blue), and the residual *SLA* change mainly due to the Bosphorus Strait outflow (red).

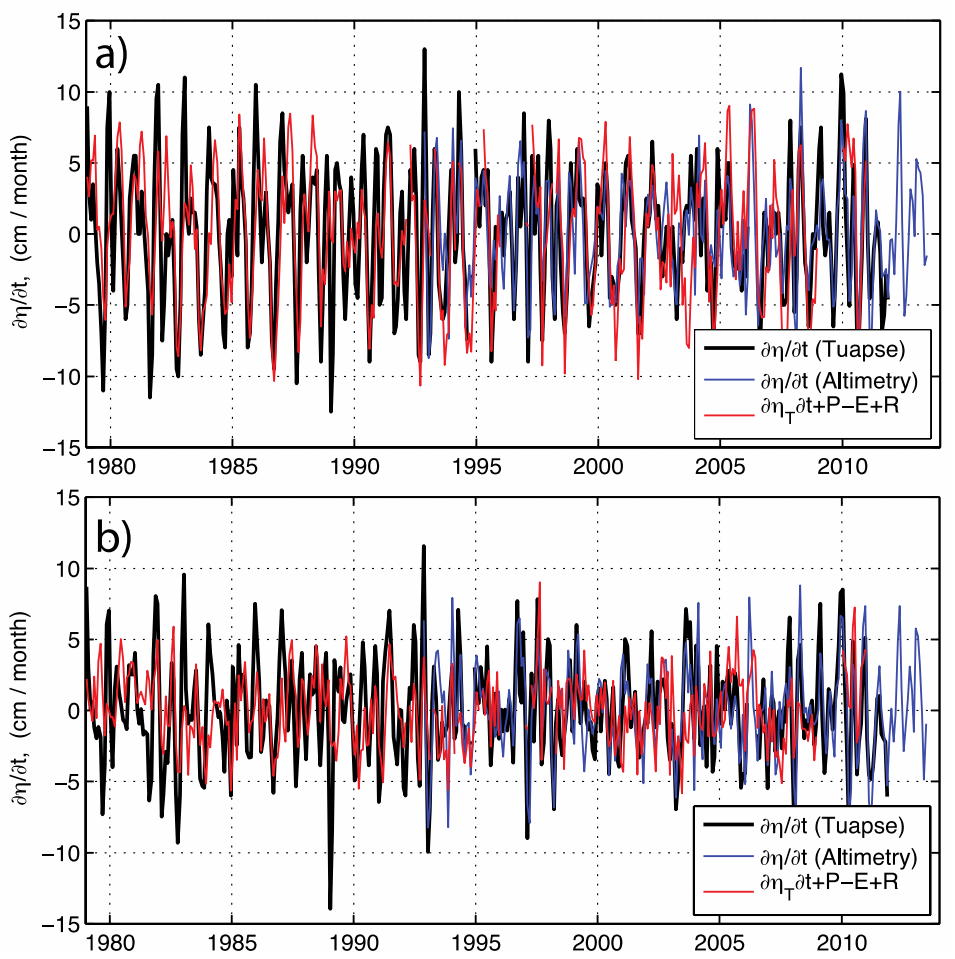

Figure 5. The time series of the time change of *SLA* components (cm/month) in the Black Sea: the total *SLA* change inferred from the Tuapse tide gauge record (black), the total *SLA* change inferred from satellite altimetry (blue), the integral *SLA* change due to surface heat flux, precipitation, evaporation and river discharge (red). (a) Seasonal cycle is present and (b) seasonal cycle is removed.

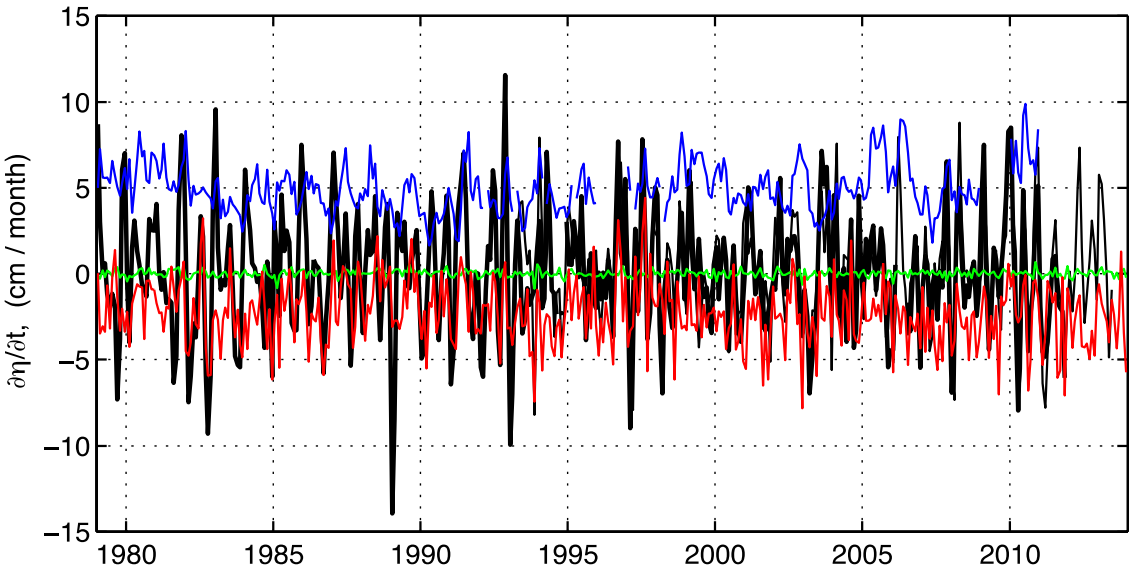

Figure 6. The time series of the time change of the nonseasonal *SLA* components in the Black Sea: the total *SLA* change inferred from the Tuapse tide gauge record (solid black), the total *SLA* change inferred from satellite altimetry (thin black), the integral *SLA* change due to precipitation and evaporation (red), the *SLA* change due to river discharge (blue) and net surface heat flux (green).

Figure 7. The yearly averages of the Danube discharge provided by GRDC and obtained using the GRACE terrestrial water storage (red curve) and the ERA-Interim terrestrial precipitation and evaporation data (black curve) over the Danube discharge area. The dots indicate data points and the dashed line is a linear interpolation to fill the 2009 gap in the GRDC data. Note that despite the bias, the combination of GRACE and ERA-Interim data captures the interannual discharge variability fairly well.

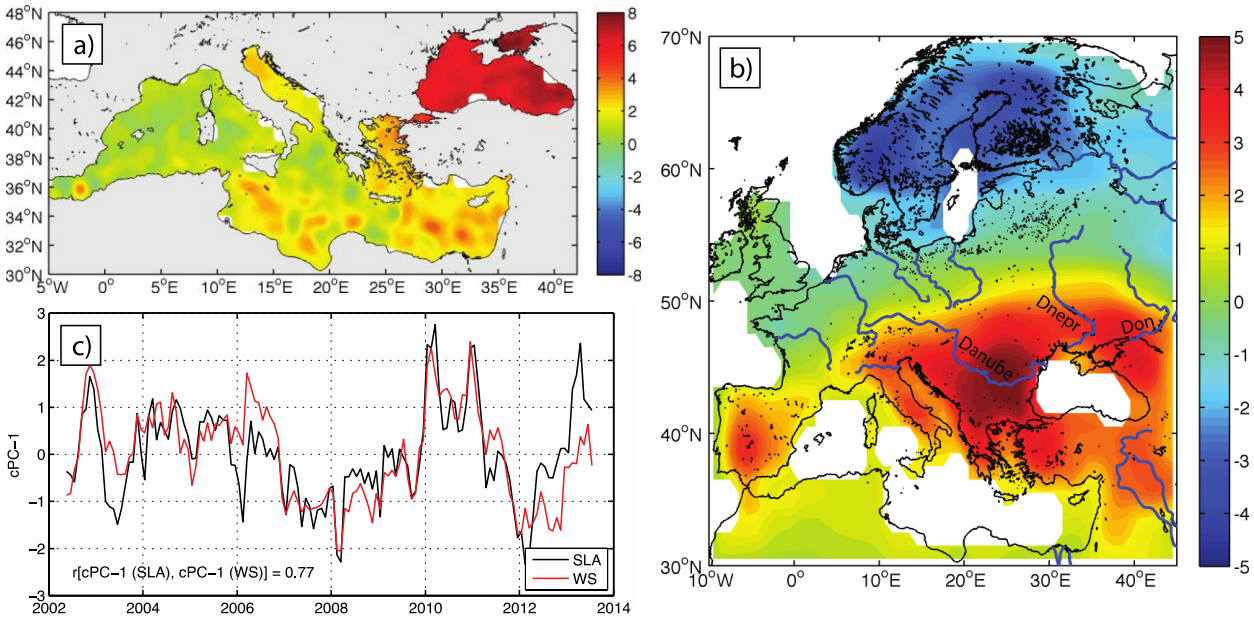

Figure 8. The cEOF-1 of satellite altimetry *SLA* and GRACE terrestrial water storage (*TWS*), shown as regression maps of (a) *SLA* and (b) *TWS* projected on (c) cPC-1 of *SLA* (black curve) and cPC-1 of *TWS* (red curve), respectively. The units are in cm per standard deviation.

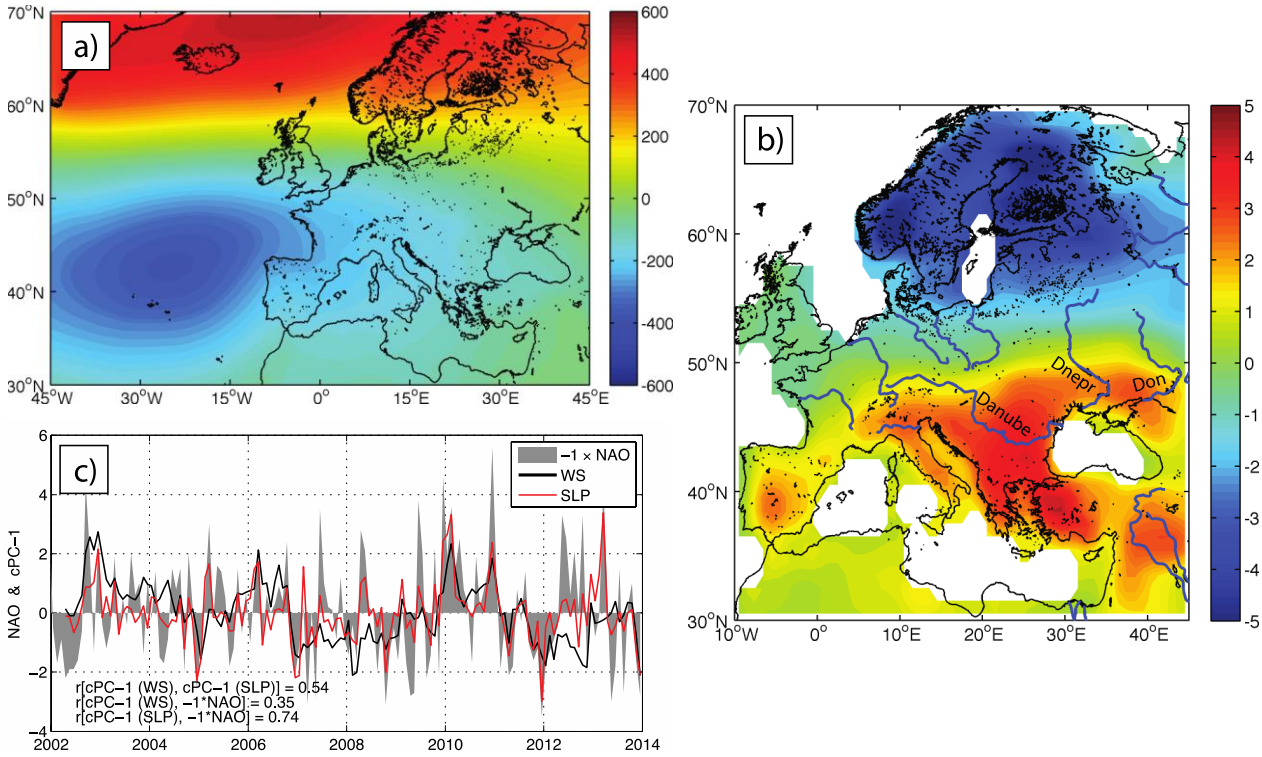

Figure 9. The cEOF-1 of ERA-Interim *SLP* and GRACE *TWS*, shown as regression maps of (a) *SLP* and (b) *S* projected on (c) cPC-1 of *SLP* (red curve) and cPC-1 of *TWS* (black curve), respectively. The units are in Pa per standard deviation for *SLP* and cm per standard deviation for *TWS*. The NAO index multiplied by –1 is shown in (c) by the gray area.

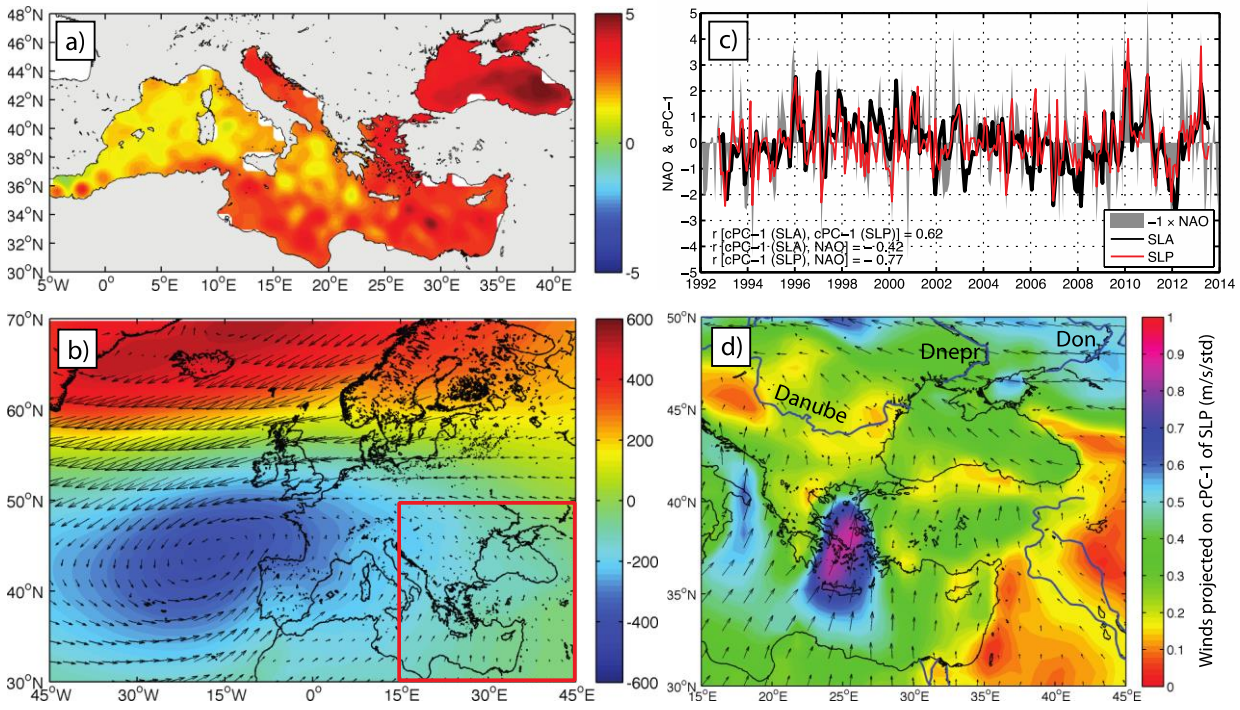

Figure 10. The cEOF-1 of satellite altimetry *SLA* and ERA-Interim *SLP*, shown as regression maps of (a) *SLA* and (b) *SLP* projected on (c) cPC-1 of *SLA* (black curve) and cPC-1 of *SLP* (red curve), respectively. The units are in cm per standard deviation for *SLA* and Pa per standard deviation for *SLP*. The NAO index multiplied by –1 is shown in (c) by the gray area. Regression map of the ERA-Interim winds projected on cPC-1 of *SLP* fields is shown by wind vectors in (b) and its zoom-in on the eastern Mediterranean and Black Sea along with the absolute wind strength (color) are shown in (d). The units of wind vectors are in m/s per standard deviation.